On the Impact of IQI on Cooperative NOMA with Direct Links in the Presence of Imperfect CSI

Safia Beddiaf[a,c], Abdellatif Khelil[a], Faical Khennoufa[a], and Khaled Rabie[b]

[a] *LEVRES Laboratory, Department of Electrical Engineering, Echahid Hamma Lakhdar University, El-Oued, Algeria.,*
[b] *Department of Engineering, Manchester Metropolitan University, Manchester M1 5GD, U.K.,*
[c] *Corresponding author: S. Beddiaf (e-mail: beddiaf-safia@univ-eloued.dz.)*

Abstract

The cooperative NOMA (CNOMA) is considered a promising technique to improve network coverage, reliability, and transmission for future wireless communication networks. However, most of the previous literature on the CNOMA ignores the RF imperfections condition. In this paper, we investigate the effect of in-phase and quadrature-phase imbalance (IQI) on CNOMA with direct links in the presence of imperfect channel state information (ICSI). The outage probability (OP) and throughput expressions are derived to evaluate the performance behaviors of the CNOMA with direct links under the IQI and ICSI imperfection. Theoretical analyzes are verified by Monte Carlo simulation. The effect of the IQI on the CNOMA with the direct links has been studied with different parameters (image rejection ratio (IRR), power allocation) and compared with conventional NOMA to clearly observe the degrading effects of imperfections on the systems. The simulation results demonstrate that the IQI and ICSI have a negative impact on the outage and throughput performance.

Keywords: IQI, imperfect CSI, outage probability, throughput, cooperative NOMA.

1. Introduction

With the rapid development of the internet of things (IoT), the beyond 5G network must support massive user and device connectivity to meet the demand for low latency, spectral efficiency and diverse service types. As a

promising solution, non-orthogonal multiple access (NOMA) gets more attention due to its ability to meet these requirements. In order to improve spectral efficiency, NOMA is integrated with a variety of techniques, including cooperative communication and multiple input multiple output (MIMO) [1, 2, 3]. In cooperative NOMA (CNOMA), there are two schemes, CNOMA without the direct links and CNOMA with the direct links. In the CNOMA scheme without the direct links, it is assumed that the users can't receive the base station (BS) signal, so it is used to extend the coverage area and help the very far users or users who suffer from channel disorders. In the CNOMA with the direct links, it is considered that the users can receive the signal from the BS and relay so the users can improve their performance by employing one of the diversity techniques (e.g., maximum ratio combining (MRC)). In order to evaluate the performance of the CNOMA without the direct links, a reversed decode-forward (DF) CNOMA under the imperfect successive interference canceler (ISIC) and imperfect channel state information (ICSI) have been analyzed in terms of the outage probability (OP) and ergodic capacity [4]. To overcomes the problems associated with poor channel quality and disconnection communication between the BS and users, the multi-hop for CNOMA to deliver the signal to the users everywhere has been performed and examined in [5]. In [6], the OP and throughput of the CNOMA over Nakagami-m fading channels were examined.

Also, to evaluate the performance of CNOMA with direct links, the authors in [7, 8] analyzed the system capacity and OP of DF relaying for CNOMA. The OP performance of the three CNOMA schemes namely, fixed relaying (FR), selective DF with coordinated direct and relay transmission (SDF-CDRT), and incremental-selective DF (ISDF), have been analyzed [9]. The incremental relay for CNOMA to improve OP performance has been examined in [10]. The authors of [11, 12] evaluate the OP and achievable rate performance of the CNOMA with and without the direct links under ICSI over the Nakagami-m fading channels. In [13], the ergodic sum-rate has been derived for CNOMA with direct links. A full-duplex (FD) and half-duplex (HD) for CNOMA with the direct links have been analyzed in terms of the OP, ergodic capacity and energy efficiency [14]. The ergodic capacity and OP for threshold-based selective CNOMA have been analyzed to provide a reliable alternative for traditional CNOMA networks [15]. The authors of [16] investigate the ergodic sum capacity and OP of the uplink CNOMA over the Rayleigh fading channel. An FD CNOMA-based coordinated direct and relay transmission has been analyzed in terms of the OP and ergodic rate

under the effect of the residual interference generated due to the ISIC [17].

On the other hand, direct-conversion transceivers are an interesting radio frequency (RF) front-end option since they do not require external intermediate frequency filters or image rejection filters [18]. Due to their high-speed data transfer, low costs and low power dissipation their architectures are assumed to be ideal candidates for wireless technologies [19]. However, in practice, the direct-conversion transceiver suffers from RF front-end-related effects due to components mismatch and imperfect manufacturing, such as in-phase and quadrature-phase imbalance (IQI). These refer to the amplitude and phase mismatch between a transceiver's I and Q branches and cause imperfect image rejection with significant performance limits [20].

The I and Q branches of the mixer in an ideal transceiver should have identical amplitude and exactly 90 phase shift, which is not realistic [21]. In practical implementations, IQI exists in the direct-conversion transceiver due to the inadequate analog components employed in the transceiver. In [22], the authors analyze the impact of IQI on the performance of different modulations under multipath fading channels. The effects of IQI on the OP of both single-carrier and multi-carrier systems cascaded Nakagami-m fading channels were evaluated [23]. The exact closed-form expression of the OP and ergodic capacity of the amplify-and-forward (AF) relay under IQI over the Nakagami-m fading channel has been derived in [24]. An FD CNOMA system under IQI and ISIC in terms of OP and ergodic sum-rate have been examined [25]. The authors in [26] examine the reliability and security of a cooperative dual-hop NOMA system in the presence of IQI. The effect of IQI and ISIC in terms of OP has been evaluated on the CNOMA system over the Nakagami-m fading channel in [27]. The OP and intercept probability (IP) have been examined for NOMA with multi-antenna under IQI over the Nakagami-m fading [28]. In [29, 30], the outage performance and ergodic rate for the ambient backscatter communication (AmBC) NOMA system with both IQI and residual hardware impairments (RHIs) has been investigated. In order to investigate the reliability and security of AmBC NOMA, the OP and the IP have been analyzed in [31, 32]. The authors in [33, 34] evaluate the error performance of downlink NOMA with the effects of IQI and ISIC.

As mentioned above, the CNOMA has been analyzed in terms of the OP, ergodic capacity in the two NOMA schemes with and without the direct links [4, 5, 6, 7, 8, 9, 10, 11, 12, 13, 14, 15, 16, 17]. All these works are considered the ideal case, so this is not practical. The RF front-end impairments are usually ignored in the literature due to their negative influence on the

CNOMA system's performance. Hence, it is important to consider this topic, considering the critical significance of this issue to the actual implementation of NOMA/CNOMA systems. The OP, ergodic capacity, and throughput for CNOMA in the presence of IQI have been evaluated in [22, 23, 24, 26]. Most of these works consider CNOMA in the presence of IQI without a direct link between the source and users due to long distances or obstacles, etc.

Correspondingly, CNOMA in the presence of IQI when the direct and relay links are available has not been considered to the best of the author's knowledge. Furthermore, all works of NOMA/CNOMA with IQI assumed the the perfect CSI [22, 23, 24, 26, 28]. The assumption of the perfect CSI is not a practical and realistic scenario. Motivated by this, our paper analyzes the effect of the IQI on the CNOMA system when the direct and relay links are available, where the ICSI is taken into consideration. In this context, the contributions of this paper are as follows:

- Since users receive signals from different sources, we consider that the MRC is used by users to combine the received signals. In this regard, we introduce a CNOMA with direct links under IQI. Also, for more realistic assumptions with the IQI effect, we have taken into account ICSI in our considered system.

- To illustrate the system's performance, we derive end-to-end (e2e) OP and throughput for our considered system under the IQI and ICSI.

- We compare our model with conventional NOMA (i.e., NOMA direct link) and we examine the impact of the image rejection ratio (IRR) and power allocation on the CNOMA/NOMA system performance. Since the distance between the relay and users affects the users' performance, we also evaluate the impact of the relay's distance on the performance of CNOMA in the presence of IQI and ICSI. Comprehensive Monte-Carlo simulation results are presented to confirm the derived expressions.

The rest of the paper is organized as follows: Section II describes the considered system model of CNOMA in the presence of IQI and ICSI. In Section III, we analyze the e2e OP and throughput of CNOMA with direct links. Section IV presents the numerical results and the conclusion is in Section V.

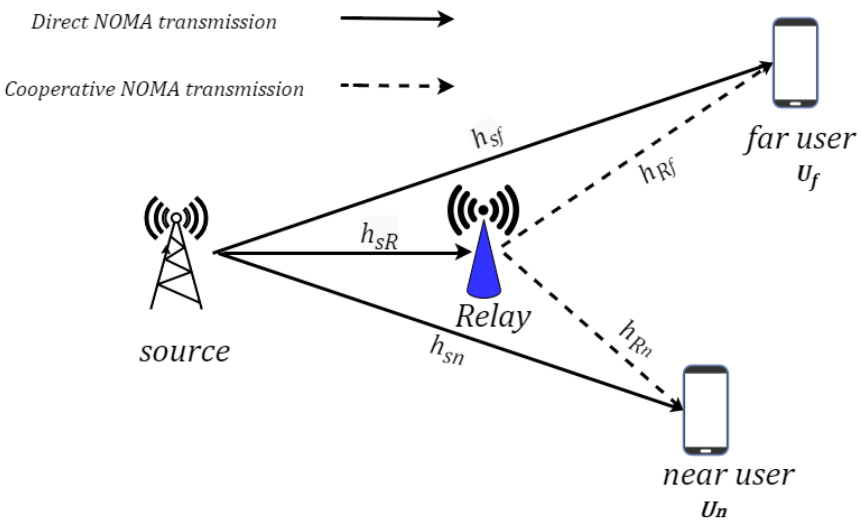

Figure 1: System model of the CNOMA with direct links.

2. System Model

We consider a downlink CNOMA scheme when the direct and relay links are available at users as presented in Fig. 1, consisting of a source (s), a DF relay (R) and two users denoted the far user U_f and near user U_n. All nodes are equipped with a single antenna and work in HD mode. The Rayleigh fading channel coefficient of the links s-users, s-R and R-users are defined by $h_i \sim \mathcal{CN}(0,\ \sigma_i^2)$, where $i = sf, sn, sR$ and $h_j \sim \mathcal{CN}(0,\ \sigma_j^2)$, where $j = Rf, Rn$. We consider that the CSI is imperfect in all links, where the estimation channels coefficients are presented as $\tilde{h}_i = h_i - \varepsilon$ and $\tilde{h}_j = h_j - \varepsilon$, where $\varepsilon \sim \mathcal{CN}(0,\ \sigma_\varepsilon^2)$ denotes the channels estimation error and we suppose it is equal in all links, $\tilde{h}_i \sim \mathcal{CN}(0,\ \sigma_i^2 - \sigma_\varepsilon^2)$ and $\tilde{h}_j \sim \mathcal{CN}(0,\ \sigma_j^2 - \sigma_\varepsilon^2)$.

The transmission occurs in two-time slots. In the first time slot, the source transmits the superimposed coding (SC) signal to users and R, $X_{sc} = \sqrt{\alpha_1}x_1 + \sqrt{\alpha_2}x_2$, where, α_1, α_2 are the power allocation coefficient for U_f and U_n messages, respectively, with $\alpha_1 > \alpha_2$, in which $\alpha_1 + \alpha_2 = 1$. x_1 and x_2 are the messages of U_f and U_n, respectively. The R/users decode x_1 and x_2, respectively using maximum likelihood detection (MLD) and SIC[1].

[1]R /U_n decodes x_1 directly using MLD by treating x_2 as noise, then decode x_2 using the SIC. While U_f decodes its signal x_1 directly using MLD.

During the second time slot, R combines the previously encoded signals in a new SC signal as in the source and forwards it to the users. U_f decodes its signal directly using MLD, while U_n uses SIC to decode its signal. As depicted in [20], the phase and/or amplitude imbalance between the in-phase (I) and quadrature-phase (Q) branches is described as IQI. Thus, the baseband representation of the IQI is defined as

$$_{IQI} = \mu_{t/r} S + \nu_{t/r} S^*, \tag{1}$$

where, S is the baseband transmit signal, $(.)^*$ is the conjugation, $\mu_{t/r}$ and $\nu_{t/r}$ are the IQI coefficients at the TX/RX respectively. We notice that, in the absence of IQI, μ_t=μ_r= 1 and ν_t=ν_r= 0. The parameter IQI are defined as [26] by $\mu_t = \frac{1}{2}(1 + \xi_t \exp(j\phi_t))$, $\nu_t = \frac{1}{2}(1 - \xi_t \exp(-j\phi_t))$, $\mu_r = \frac{1}{2}(1 + \xi_r \exp(-j\phi_r))$ and $\nu_r = \frac{1}{2}(1 - \xi_r \exp(j\phi_r))$,

with $\xi_{t/r}$ and $\phi_{t/r}$ are the gain and the phase imbalances levels of TX/RX, j is the unit of the imaginary $j = \sqrt{-1}$. Furthermore, IRR[2] is given

$$IRR_{t/r} = \frac{|\ \mu_{t/r}|^2}{|\ \nu_{t/r}|^2}. \tag{2}$$

At the first time slot, according to the NOMA protocol, we consider the presence of IQI in both of TX and RX. The received signal with ICSI is given as

$$\begin{aligned} y_i{}^{IQI} &= \mu_{r,i}((\tilde{h}_i + \varepsilon)\sqrt{P_s}(\mu_{t,i} X_{sc} + \nu_{t,i} X_{sc}{}^*) + n_i) \\ &+ \nu_{r,i}((\tilde{h}_i + \varepsilon)\sqrt{P_s}(\mu_{t,i} X_{sc} + \nu_{t,i} X_{sc}{}^*) + n_i)^*,\ i = sf, sn, sR, \end{aligned} \tag{3}$$

where P_s is the transmit power of the source. n_i is the additive white Gaussian noise (AWGN) with $CN(0,\ N_0)$, $\mu_{t,i/r,i}$ and $\nu_{t,i/r,i}$ are the IQI coefficients at the TX/RX and equal to $\mu_{t/r}$ and $\nu_{t/r}$ in (1).

Assuming the ICSI, the received signal-to-interference-plus noise ratio (SINR) of the x_1 at the first time slot (i.e., at R, U_f and U_n) is given by

$$\gamma_{sf} = \frac{\Delta_{1,sf}\alpha_1\lambda_s|\tilde{h}_{sf}|}{\Delta_{1,sf}\alpha_2\lambda_s|\tilde{h}_{sf}| + \Delta_{1,sf}\lambda_s\sigma_\varepsilon^2 + \Delta_{2,sf}\lambda_s|\tilde{h}_{sf}| + \Delta_{2,sf}\lambda_s\sigma_\varepsilon^2 + \Delta_{3,sf}}, \tag{4}$$

[2]The IRR measures the amount of attenuation of the image frequency band. The IRR is typically in the range of 20 to 40 dB for useful analog RF front-end circuits [18, 19, 35, 36, 37, 38].

$$\gamma_{sn\to sf} = \frac{\Delta_{1,sn}\alpha_1\lambda_s|\tilde{h}_{sn}|}{\Delta_{1,sn}\alpha_2\lambda_s|\tilde{h}_{sn}| + \Delta_{1,sn}\lambda_s\sigma_\varepsilon^2 + \Delta_{2,sn}\lambda_s|\tilde{h}_{sn}| + \Delta_{2,sn}\lambda_s\sigma_\varepsilon^2 + \Delta_{3,sn}}, \tag{5}$$

$$\gamma_{sR}{}^{U_f} = \frac{\Delta_{1,sR}\alpha_1\lambda_s|\tilde{h}_{sR}|}{\Delta_{1,sR}\alpha_2\lambda_s|\tilde{h}_{sR}| + \Delta_{1,sR}\lambda_s\sigma_\varepsilon^2 + \Delta_{2,sR}\lambda_s|\tilde{h}_{sR}| + \Delta_{2,sR}\lambda_s\sigma_\varepsilon^2 + \Delta_{3,sR}}. \tag{6}$$

In contrast, U_n and R cancel the x_1 signal's using the SIC process to detect x_2 signal, so the SINR of the x_2 at U_n and R by assuming a perfect SIC and ICSI is defined as

$$\gamma_{sn} = \frac{\Delta_{1,sn}\alpha_2\lambda_s|\tilde{h}_{sn}|}{\Delta_{1,sn}\lambda_s\sigma_\varepsilon^2 + \Delta_{2,sn}\alpha_2\lambda_s|\tilde{h}_{sn}| + \Delta_{2,sn}\lambda_s\sigma_\varepsilon^2 + \Delta_{3,sn}}, \tag{7}$$

$$\gamma_{sR}{}^{U_n} = \frac{\Delta_{1,sR}\alpha_2\lambda_s|\tilde{h}_{sR}|}{\Delta_{1,sR}\lambda_s\sigma_\varepsilon^2 + \Delta_{2,sR}\alpha_2\lambda_s|\tilde{h}_{sR}| + \Delta_{2,sR}\lambda_s\sigma_\varepsilon^2 + \Delta_{3,sR}}, \tag{8}$$

where $\Delta_{1,i} = \mu_{t,i}^2\mu_{r,i}^2 + \nu_{t,i}^2\nu_{r,i}^2$, $\Delta_{2,i} = \mu_{r,i}^2\nu_{t,i}^2 + \nu_{r,i}^2\mu_{t,i}^2$, $\Delta_{3,i} = \mu_{r,i}^2 + \nu_{r,i}^2$ and λ_s is the transmit signal to noise ratio (SNR) by the source $\lambda_s = \frac{P_s}{N_0}$.

Likewise, in the second time slot, we assume that both users are affected by the IQI and ICSI. However, the received signal at U_f and U_n can be expressed as

$$\begin{aligned} y_j{}^{IQI} =& \mu_{r,j}((\tilde{h}_j + \varepsilon)\sqrt{P_R}(\mu_{t,j}X_{sc} + \nu_{t,j}{X_{sc}}^*) + n_j) + \nu_{r,j}((\tilde{h}_j + \varepsilon) \\ & \times \sqrt{P_R}(\mu_{t,j}X_{sc} + \nu_{t,j}{X_{sc}}^*) + n_j)^*,\ j = Rn, Rf, \end{aligned} \tag{9}$$

where P_R transmit power of R, n_j is the AWGN with $CN(0,\ N_0)$, $\mu_{t,j/r,j}$ and $\nu_{t,j/r,j}$ are the IQI coefficients at the TX/RX and equal to $\mu_{t/r}$ and $\nu_{t/r}$ in (1).

The received SINR at U_f and U_n to decode the signal x_1 is presented respectively as

$$\gamma_{Rf} = \frac{\Delta_{1,Rf}\alpha_1\lambda_R|\tilde{h}_{Rf}|}{\Delta_{1,Rf}\alpha_2\lambda_R|\tilde{h}_{Rf}| + \Delta_{1,Rf}\lambda_R\sigma_\varepsilon^2 + \Delta_{2,Rf}\lambda_R|\tilde{h}_{Rf}| + \Delta_{2,Rf}\lambda_R\sigma_\varepsilon^2 + \Delta_{3,Rf}}, \tag{10}$$

$$\gamma_{Rn\to Rf} = \frac{\Delta_{1,Rn}\alpha_1\lambda_R|\tilde{h}_{Rn}|}{\Delta_{1,Rn}\alpha_2\lambda_R|\tilde{h}_{Rn}| + \Delta_{1,Rn}\lambda_R\sigma_\varepsilon^2 + \Delta_{2,Rn}\lambda_R|\tilde{h}_{Rn}| + \Delta_{2,Rn}\lambda_R\sigma_\varepsilon^2 + \Delta_{3,Rn}}. \tag{11}$$

The U_n use the SIC process to cancel the interference created by the x_1 signal. Thus, assuming a perfect cancellation, the received SINR at U_n is obtained as

$$\gamma_{Rn} = \frac{\Delta_{1,Rn}\alpha_2\lambda_R|\tilde{h}_{Rn}|}{\Delta_{1,Rn}\lambda_R\sigma_\varepsilon^2 + \Delta_{2,Rn}\alpha_2\lambda_R|\tilde{h}_{Rn}| + \Delta_{2,Rn}\lambda_R\sigma_\varepsilon^2 + \Delta_{3,Rn}}, \tag{12}$$

where $\Delta_{1,j} = \mu_{t,j}^2\mu_{r,i}^2 + \nu_{t,j}^2\nu_{r,j}^2$, $\Delta_{2,j} = \mu_{r,j}^2\nu_{t,j}^2 + \nu_{r,j}^2\mu_{t,j}^2$, $\Delta_{3,j} = \mu_{r,j}^2 + \nu_{r,j}^2$ and λ_R is the transmit SNR by R $\lambda_R = \frac{P_R}{N_0}$. The U_n and U_f receive two signals from the source and R. Thus, we assume that the U_f and U_n implement the MRC to combine the two received signals.

3. Performance Analysis of the System

In this section, we derive the e2e OP and throughput expressions of our considered system in the presence of IQI and ICSI.

3.1. Outage probability

The outage is the event when the user/node cannot reliably decode the received signal i.e., the capacity is less than the target rate. The OP expression of U_f using the MRC is given as [39] by

$$\begin{aligned} P_{out,u_f} =& (1 - P({\gamma_{sR}}^{U_f} < \theta_1))P(\gamma_{sf} + \gamma_{Rf} < \theta_1) \\ &+ P({\gamma_{sR}}^{U_f} < \theta_1)P(\gamma_{sf} < \theta_1), \end{aligned} \tag{13}$$

where $\theta_1 = 2^{2R1} - 1$ is the threshold to detect x_1, $R1$ is the target rate of x_1. $P({\gamma_{sR}}^{U_f} < \theta_1)$ is the OP of x_1 at R, $P(\gamma_{sf} < \theta_1)$ is the OP of x_1 at U_f, $P(\gamma_{sf} + \gamma_{Rf} < \theta_1)$ is the OP of x_1 at U_f when MRC is implemented. Each term of (13) is calculated as

$$P(\gamma_{sf} < \theta_1) = 1 - \exp\left(-\tau_1\theta_1\right), \tag{14}$$

$$P(\gamma_{sR}^{U_f} < \theta_1) = 1 - \exp\left(-\tau_2\theta_1\right), \tag{15}$$

where $\tau_1 = \frac{(\Delta_{3,sf}+\Delta_{2,sf}\lambda_s\sigma_\varepsilon^2+\Delta_{1,sf}\lambda_s\sigma_\varepsilon^2)}{\varphi_{sf}(\Delta_{1,sf}\alpha_1-\Delta_{1,sf}\alpha_2\theta_1-\Delta_{2,sf}\theta_1)\lambda_s}$, $\tau_2 = \frac{(\Delta_{3,sR}+\Delta_{2,sR}\lambda_s\sigma_\varepsilon^2+\Delta_{1,sR}\lambda_s\sigma_\varepsilon^2)}{\varphi_{sR}(\Delta_{1,sR}\alpha_1-\Delta_{1,sR}\alpha_2\theta_1-\Delta_{2,sR}\theta_1)\lambda_s}$, $\varphi_{sf} = E[|\tilde{h}_{sf}|^2], \varphi_{sR} = E[|\tilde{h}_{sR}|^2]$ and $E[.]$ is the expectation operator.

To evaluate P_{out,u_f}, it is important to get the distribution of $\gamma_{sf}+\gamma_{Rf}$. In general, for two independent exponential random variables X and Y, when X $\neq$ Y, the CDF of two independent exponential random variables Z=X+Y can be computed as [39, eq. (6)] by

$$\begin{aligned} &P(X+Y<k) = \\ &1-\left[\frac{X}{X-Y}\exp\left(-\frac{X}{Y}\right)+\frac{X}{Y-X}\exp\left(-\frac{K}{Y}\right)\right] X \neq Y. \end{aligned} \tag{16}$$

Since γ_{sf} and γ_{Rf} are two independent exponential random variables, where $\gamma_{sf} \neq \gamma_{Rf}$, so $P(\gamma_{sf}+\gamma_{Rf} < R1)$ can be computed as (16) by

$$P(\gamma_{sf}+\gamma_{Rf}<\theta_1) = 1-\left[\frac{\tau_1}{\tau_1-\tau_3}\exp\left(-\tau_1\theta_1\right)+\frac{\tau_3}{\tau_3-\tau_1}\exp\left(\tau_3\theta_1\right)\right] \tau_1 \neq \tau_3, \tag{17}$$

where $\tau_3 = \frac{(\Delta_{3,Rf}+\Delta_{2,Rf}\lambda_s\sigma_\varepsilon^2+\Delta_{1,Rf}\lambda_s\sigma_\varepsilon^2)}{\varphi_{Rf}(\Delta_{1,Rf}\alpha_1-\Delta_{1,Rf}\alpha_2\theta_1-\Delta_{2,Rf}\theta_1)\lambda_s}$.

By substituting (14), (15) and (17) into (13), we find the OP of U_f as expressed by

$$\begin{aligned} P_{out,u_f} =& \exp\left(-\tau_2\theta_1\right)\left(1-\left[\frac{\tau_1}{\tau_1-\tau_3}\exp\left(-\tau_1\theta_1\right)+\frac{\tau_3}{\tau_3-\tau_1}\exp\left(\tau_3\theta_1\right)\right]\right)+ \\ &\left(1-\exp\left(-\tau_2\theta_1\right)\right)\left(1-\exp\left(-\tau_1\theta_1\right)\right). \end{aligned} \tag{18}$$

When MRC is implemented at U_n, the detection of x_2 is based on if the U_n is able or not to detect x_1. Thus, the OP occurs at the U_n at output MRC to detect x_2 is given as

$$P_{out,U_n} = P_{out,U_n\to U_f}^{MRC} + \left[1-P_{out,U_n\to U_f}^{MRC}\right] P_{out,U_n}^{MRC}, \tag{19}$$

where $P_{out,U_n\to U_f}^{MRC}$ is the OP at output MRC to detect x_1 at U_n and P_{out,U_n}^{MRC} is the OP at output MRC after implementing the SIC at U_n to detect x_2. Each term of (19) is calculated below.

The U_n receives two signals from different sources one from the source and the other from R. The U_n implements MRC to combine the two received signals. After MRC is implemented, the U_n detect x_1 firstly. Thus, the OP to detect x_1 at U_n at output MRC is expressed as

$$\begin{aligned} P_{out,U_n\to U_f}^{MRC} =&(1-P\left({\gamma_{sR}}^{U_f}<\theta_1\right))P\left(\gamma_{sn\to sf}+\gamma_{Rn\to Rf}<\theta_1\right) \\ &+P\left({\gamma_{sR}}^{U_f}<\theta_1\right)P\left(\gamma_{sn\to sf}<\theta_1\right), \end{aligned} \tag{20}$$

where $P\left(\gamma_{sn\to sf}+\gamma_{Rn\to Rf}<\theta_1\right)$ is the OP of x_1 at U_n when MRC is implemented, $P\left(\gamma_{sn\to sf}<\theta_1\right)$ is the OP of the direct link of x_1 at U_n. Each term of (20) is calculated as

$$P\left(\gamma_{sn\to sf}<\theta_1\right)=1-\exp\left(-\tau_4\theta_1\right), \tag{21}$$

$$\begin{aligned} &P(\gamma_{sn\to sf}+\gamma_{Rn\to Rf}<\theta_1)= \\ &1-\left[\frac{\tau_4}{\tau_4-\tau_5}\exp\left(-\tau_4\theta_1\right)+\frac{\tau_5}{\tau_5-\tau_4}\exp\left(\tau_5\theta_1\right)\right]\tau_4\neq\tau_5, \end{aligned} \tag{22}$$

where $\tau_4=\frac{(\Delta_{3,sn}+\Delta_{2,sn}\lambda_s\sigma_\varepsilon^2+\Delta_{1,sn}\lambda_s\sigma_\varepsilon^2)}{\varphi_{sn}(\Delta_{1,sn}\alpha_1-\Delta_{1,sn}\alpha_2\theta_1-\Delta_{2,sn}\theta_1)\lambda_s}$, $\tau_5=\frac{(\Delta_{3,Rn}+\Delta_{2,Rn}\lambda_s\sigma_\varepsilon^2+\Delta_{1,Rn}\lambda_s\sigma_\varepsilon^2)}{\varphi_{Rn}(\Delta_{1,Rn}\alpha_1-\Delta_{1,sn}\alpha_2\theta_1-\Delta_{2,Rn}\theta_1)\lambda_s}$.

By substituting (15), (21) and (22) into (20), we get the OP of x_1 at U_n at output MRC as given by

$$\begin{aligned} P_{out,U_n\to U_f}^{MRC} =&\exp\left(-\tau_2\theta_1\right)\left(1-\left[\frac{\tau_4}{\tau_4-\tau_5}\exp\left(-\tau_4\theta_1\right)+\frac{\tau_5}{\tau_5-\tau_4}\exp\left(\tau_5\theta_1\right)\right]\right)+ \\ &\left(1-\exp\left(-\tau_2\theta_1\right)\right)\left(1-\exp\left(-\tau_4\theta_1\right)\right). \end{aligned} \tag{23}$$

Thereafter, U_n using the SIC detect its signal x_2. The OP of x_2 at U_n at output MRC can be expressed by

$$\begin{aligned} P_{out,u_n}^{MRC} =&(1-P({\gamma_{sR}}^{U_n}<\theta_2))P(\gamma_{sn}+\gamma_{Rn}<\theta_2) \\ &+P({\gamma_{sR}}^{U_n}<\theta_2)P(\gamma_{sn}<\theta_2), \end{aligned} \tag{24}$$

where $\theta_2=2^{2R2}-1$ is the threshold to detect x_2, $R2$ is the target rate to detect x_2, $P(\gamma_{sn}<\theta_2)$ is the OP of direct link of x_2 at U_n, $P(\gamma_{sn}+\gamma_{Rn}<\theta_2)$

is the OP of x_2 at U_n when MRC is implemented, $P({\gamma_{sR}}^{U_n} < \theta_2)$ is the OP to detect x_2 at R. Each term of (24) is calculated as

$$P(\gamma_{sn} < \theta_2) = 1 - \exp\left(-\tau_6\theta_2\right), \tag{25}$$

$$P(\gamma_{sR}^{U_n} < \theta_2) = 1 - \exp\left(-\tau_7\theta_2\right), \tag{26}$$

$$P(\gamma_{sn} + \gamma_{Rn} < \theta_2) = 1 - \left[\frac{\tau_8}{\tau_8 - \tau_6}\exp\left(-\tau_8\theta_2\right) + \frac{\tau_6}{\tau_6 - \tau_8}\exp\left(\tau_6\theta_2\right)\right] \tau_8 \neq \tau_6, \tag{27}$$

where $\tau_6 = \frac{(\Delta_{3,sn}+\Delta_{2,sn}\lambda_s\sigma_\varepsilon^2+\Delta_{1,sn}\lambda_s\sigma_\varepsilon^2)\theta_2}{\varphi_{sn}(\Delta_{1,sn}\alpha_2\theta_2-\Delta_{2,sn}\theta_2)\lambda_s}$, $\tau_7 = \frac{(\Delta_{3,sR}+\Delta_{2,sR}\lambda_s\sigma_\varepsilon^2+\Delta_{1,sR}\lambda_s\sigma_\varepsilon^2)\theta_2}{\varphi_{sR}(\Delta_{1,sR}\alpha_2\theta_2-\Delta_{2,sR}\theta_2)\lambda_s}$, $\varphi_{sn} = E[|\tilde{h}_{sn}|^2]$, $\tau_8 = \frac{(\Delta_{3,Rn}+\Delta_{2,Rn}\lambda_s\sigma_\varepsilon^2+\Delta_{1,Rn}\lambda_s\sigma_\varepsilon^2)}{\varphi_{Rn}(\Delta_{1,Rn}\alpha_2\theta_2-\Delta_{2,Rn}\theta_2)\lambda_s}$.

Thus, substituting (25), (26) and (27) into (24) to find the OP of x_2 at U_n at output MRC, we obtain

$$\begin{aligned} P_{out,U_n}^{MRC} =& \exp\left(-\tau_7\theta_2\right)\left(1 - \left[\frac{\tau_8}{\tau_8 - \tau_6}\exp\left(-\tau_8\theta_2\right) + \frac{\tau_6}{\tau_6 - \tau_8}\exp\left(\tau_6\theta_2\right)\right]\right) + \\ & (1 - \exp\left(-\tau_7\theta_2\right))(1 - \exp\left(-\tau_6\theta_2\right)). \end{aligned} \tag{28}$$

As we described above, the OP of U_n at the output MRC occurs in two events as given in (19): If the received SINR of x_1 at the output MRC is unsuccessfully detected and if the received SINR of x_1 at the output MRC is successfully detected and fails to detect x_2 at the output MRC. Hence, we find the OP of U_n at output MRC by substituting (23) and (28) into (19).

3.2. Throughput

In this subsection, we present the throughput of our considered systems. Thus, the throughput is expressed as

$$\tau = (1 - P_{out,U_n})R2 + (1 - P_{out,U_f})R1, \tag{29}$$

where P_{out,U_n} and P_{out,U_f} are the OP of U_n and U_f respectively at output MRC and are obtained in (18) and (19).

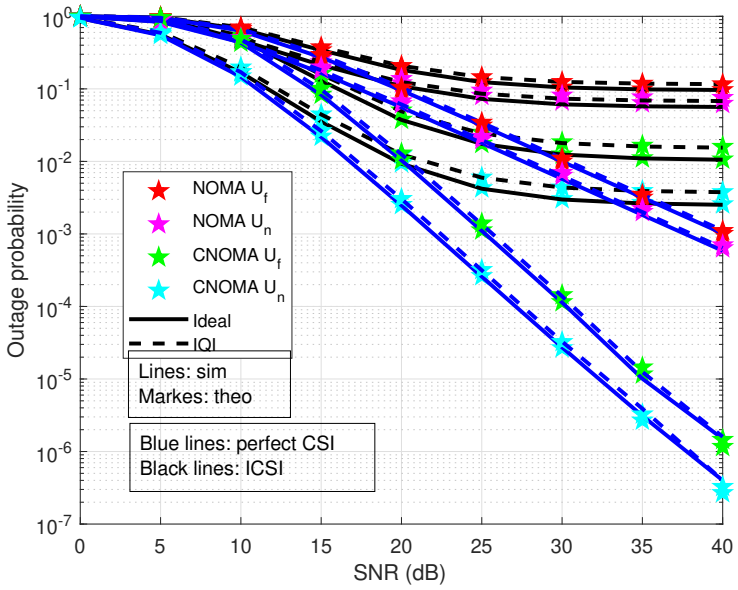

Figure 2: OP of CNOMA w.r.t SNR when IRR=20dB

4. Numerical Results

In this section, the performance of the CNOMA with direct links in the presence of the IQI and ICSI is evaluated in terms of the OP and throughput with a comparison with NOMA. The analytical results have been validated through the simulation results. In the results, the lines represent the simulation results, and the marks represent the theoretical results. The simulation results are matched perfectly with the numerical results. The parameters used in the simulations are set to d_{sf}=5m, d_{sn}=2m, d_{sR}=1m, d_{Rf}=4m, d_{Rf}=1m, $\alpha_1 = 0.9$, α_2=0.1, σ_ε^2=0, 0.01 and path loss factor is equal to 3. In all simulation results, we consider that IRR=IRR_t=IRR_r and P_s=P_R.

Fig. 2 presents the OP of the CNOMA versus SNR under ideal, IQI and ICSI conditions, when R1=R2=0.1. We observe that the OP of CNOMA is superior to NOMA for both users with ideal/non-ideal IQI and with/without ICSI. Furthermore, it can be easily observed that the OP of the users with ideal IQI outperforms the non-ideal condition. The ICSI degraded the OP performance at high SNR in both users. Therefore, increasing SNR in the presence of ICSI does not improve the system performance.

In Fig. 3, we illustrate the OP of the CNOMA in the function of IRR,

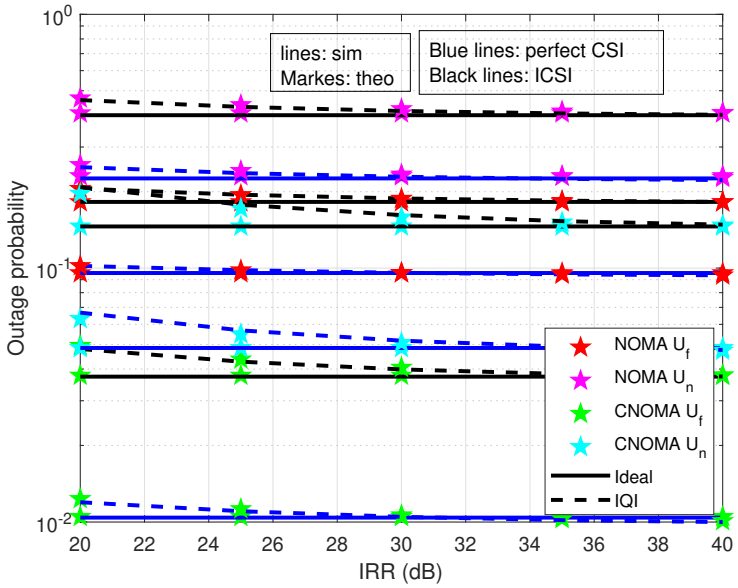

Figure 3: OP of CNOMA w.r.t IRR when SNR=20dB

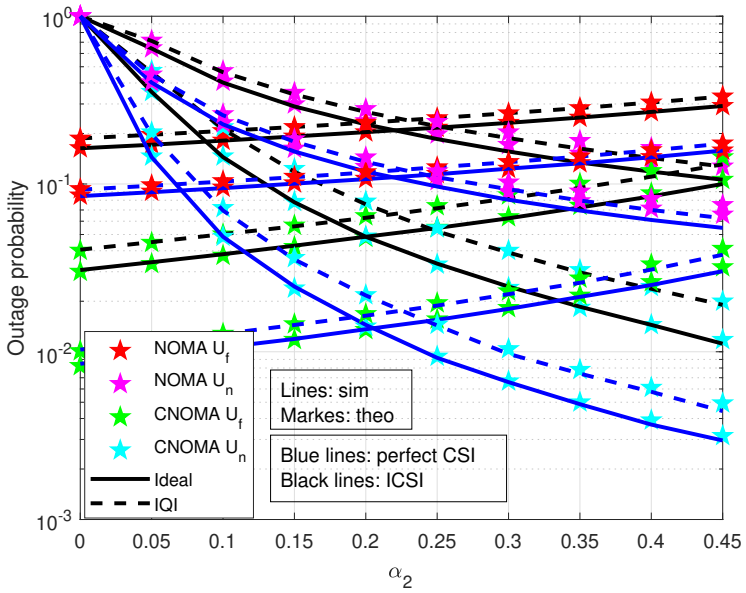

Figure 4: OP of CNOMA w.r.t α_2 when IRR=20dB.

when SNR= 20 dB, R1= 0.1 and R2 = 0.4. It can be easily seen that the OP of the users improves with the increase of IRR and is almost identical to those of the perfect case (without IQI) for the high IRR. Also, the presence of the ICSI deteriorates the OP performance in ideal and non-ideal IQI. Additionally, in this figure, depending on the gaps between the perfect IQ matching and IQI curves, the IQI has various effects on the OP performance of different users in the considered system. Therefore, these findings highlight the negative effects of IQI and demonstrate the significance of taking RF impairments into account.

Also, in order to show the effect of power allocation in the presence of the IQI and ICSI, Fig. 4 presents the OP versus power allocation (α_2), when R1=0.1 and R2=0.4. We observe that increasing α_2 degrades the performance of one user at the expense of the other in ideal/non-ideal IQI and with/without ICSI. The presence of IQI and ICSI degrades OP performance. Thus, the system performance under imperfection depends on the power allocation coefficient, which indicates the importance of power allocation in the RF and ICSI impairment.

The effect of IQ imbalance is evaluated for the throughput performance and presented in Fig. 5, when $\sigma_\epsilon^2 = 0, 0.01$, IRR= 20 dB and R1=R2=0.1. It can be observed that CNOMA increases the throughput performance of NOMA for ideal/non-ideal IQI and with/withoutICSI. Also, the throughput of the ideal IQI achieves a higher performance gain compared to the non-ideal condition. The ICSI degraded the throughput performance in ideal and non-ideal IQI.

In Fig. 6, we illustrate the throughput of the CNOMA w.r.t IRR, when SNR=20 dB, R1= 0.1 and R2= 0.4. We observe that the CNOMA improves the throughput of NOMA for ideal/non-ideal and with/without ICSI. It can be seen that the throughput of NOMA/CNOMA increases with the increase of IRR and is almost identical to those of the perfect case (without IQI) for the high IRR. Furthermore, the presence of ICSI degrades the throughput performance for ideal and non-ideal IQI conditions. The error of signal detection is increased when IQI and ICSI are present. Thus, these results illustrate the detrimental impacts of IQI on throughput performance and show the importance of considering RF impairments.

In order to show the impact of R distance on the throughput performance of CNOMA in the presence of IQI and ICSI, Fig. 7 presents the throughput of the CNOMA w.r.t R distance, when IRR=SNR= 20 dB, R1=0.1 and R2=0.4. We observe that the increasing distance improves the throughput

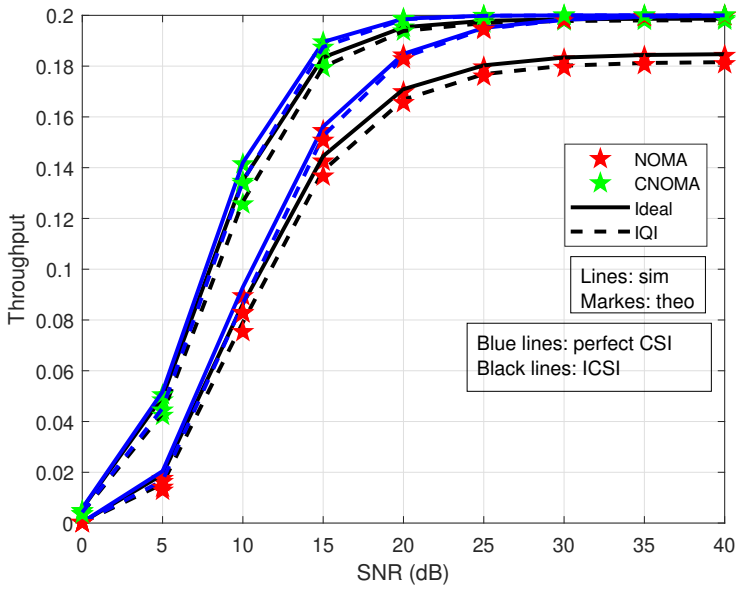

Figure 5: Throughput of CNOMA w.r.t SNR when IRR=20dB

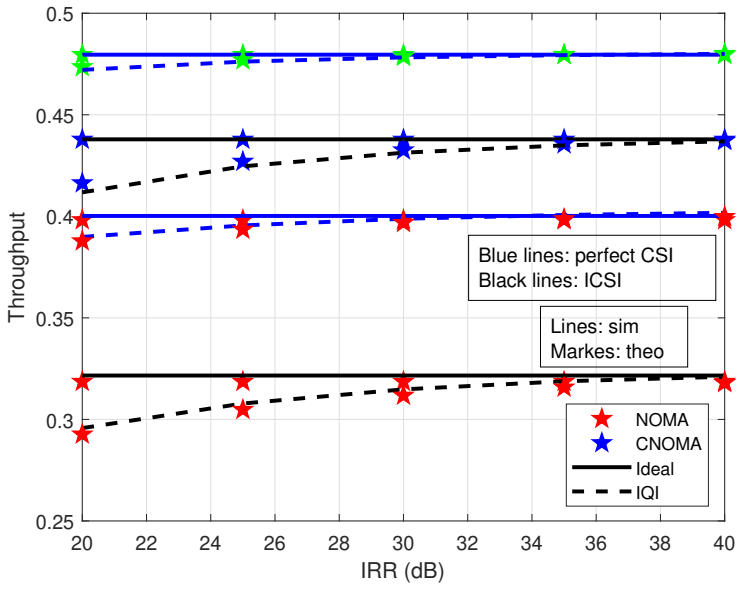

Figure 6: Throughput of CNOMA w.r.t IRR when SNR=20dB

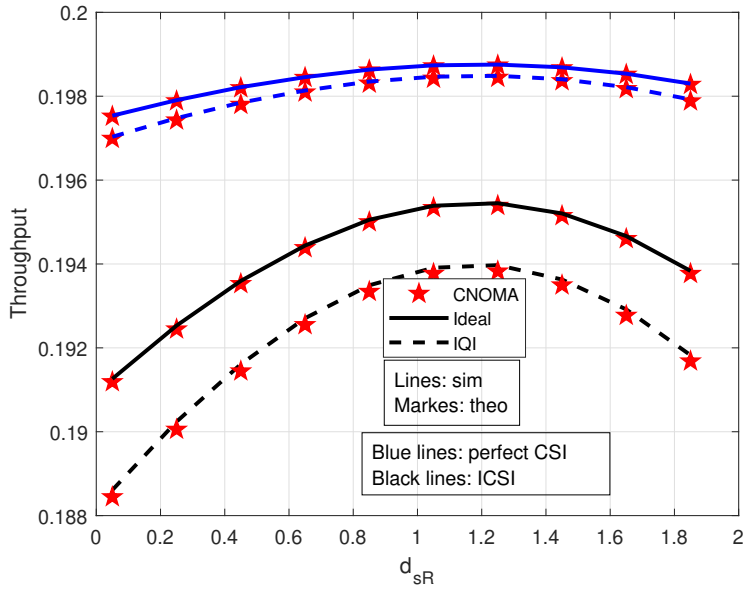

Figure 7: Throughput of CNOMA w.r.t d_{sR} when IRR=SNR=20dB.

performance with ideal/non-ideal IQI, and perfect CSI and ICSI. The higher distance between the source and R degrades the throughput performance. Increasing the distance between the source and R degrade the throughput performance, and this also means more error in the signal detection at the R. Therefore, the information forwarding in the second phase will be with more error.

5. Conclusion

In this paper, we investigate the performance of IQI on the CNOMA with direct links in the presence of ICSI. We derive the OP and throughput expressions to evaluate the effect of imperfections on the performance of the systems. The effects of IQI and ICSI are examined on the CNOMA with direct links and compared to the conventional NOMA. The mathematical analyzes were validated using the simulation results. The results revealed that joint imperfections degrade significantly the performance of the systems. The presence of ICSI degrades the performance of the ideal and non-ideal IQI. To this end, it is crucial to apply an efficient model, optimization, and

dynamic compensation for the implementation of the NOMA and CNOMA systems.

References

[1] Z. Wang, Z. Peng, Y. Pei, H. Wang, Performance analysis of cooperative NOMA systems with incremental relaying, Wirel. Commun. Mob. Comp. 2020 (2020).

[2] X. Li, M. Liu, C. Deng, D. Zhang, X.-C. Gao, K. M. Rabie, R. Kharel, Joint effects of residual hardware impairments and channel estimation errors on SWIPT assisted cooperative NOMA networks, IEEE Access 7 (2019) 135499–135513.

[3] T. M. C. Chu, H.-J. Zepernick, Outage probability and secrecy capacity of a non-orthogonal multiple access system, in: 2017 11th International Conference on Signal Processing and Communication Systems (ICSPCS), IEEE, 2017, pp. 1–6.

[4] F. Kara, H. Kaya, Improved user fairness in decode-forward relaying non-orthogonal multiple access schemes with imperfect SIC and CSI, IEEE Access 8 (2020) 97540–97556.

[5] F. Khennoufa, K. Abdellatif, F. Kara, Bit error rate and outage probability analysis for multi-hop decode-and-forward relay-aided NOMA with imperfect SIC and imperfect CSI, AEU-Intern. J. Elec. Commun. 147 (2022) 154124.

[6] S. M. Ibraheem, W. Bedawy, W. Saad, M. Shokair, Outage performance of NOMA-based DF relay sharing networks over Nakagami-m fading channels, in: 2018 13th Intern. Conf. Comp. Eng. Sys. (ICCES), IEEE, 2018, pp. 512–517.

[7] J.-B. Kim, I.-H. Lee, Non-orthogonal multiple access in coordinated direct and relay transmission, IEEE Commun. Lett. 19 (11) (2015) 2037–2040.

[8] G. Nauryzbayev, O. Omarov, S. Arzykulov, K. M. Rabie, X. Li, A. M. Eltawil, Performance limits of wireless powered cooperative NOMA over generalized fading, Trans. Emerg. Telecommun. Tech. 33 (4) (2022) e4415.

[9] H. Liu, Z. Ding, K. J. Kim, K. S. Kwak, H. V. Poor, Decode-and-forward relaying for cooperative NOMA systems with direct links, IEEE Trans. Wirel.Commun. 17 (12) (2018) 8077–8093.

[10] G. Li, D. Mishra, H. Jiang, Cooperative NOMA with incremental relaying: Performance analysis and optimization, IEEE Transactions on Vehicular Technology 67 (11) (2018) 11291–11295.

[11] X. Gong, X. Yue, F. Liu, Performance analysis of cooperative NOMA networks with imperfect CSI over Nakagami-m fading channels, Sensors 20 (2) (2020) 424.

[12] J. Zhang, L. Dai, R. Jiao, X. Li, Y. Liu, Performance analysis of relay assisted cooperative non-orthogonal multiple access systems, submitted to IEEE Wireless Commun. Lett (2017).

[13] W. Duan, G. Zhang, Q. Sun, J. Hou, Y. Ji, J. Choi, On the performance of an enhanced transmission scheme for cooperative relay networks with NOMA, EURASIP Journal on Wireless Communications and Networking 2018 (1) (2018) 1–14.

[14] X. Yue, Y. Liu, S. Kang, A. Nallanathan, Z. Ding, Exploiting full/half-duplex user relaying in NOMA systems, IEEE Transactions on Communications 66 (2) (2017) 560–575.

[15] F. Kara, H. Kaya, Threshold-based selective cooperative NOMA: Capacity/outage analysis and a joint power allocation-threshold selection optimization, IEEE Communications Letters 24 (9) (2020) 1929–1933.

[16] M. B. Uddin, M. F. Kader, S. Y. Shin, Uplink cooperative diversity using power-domain nonorthogonal multiple access, Transactions on Emerging Telecommunications Technologies 30 (12) (2019) e3678.

[17] Y. Zhang, Z. Yang, Y. Feng, S. Yan, Performance analysis of a novel uplink cooperative NOMA system with full-duplex relaying, IET Communications 12 (19) (2018) 2408–2417.

[18] A. A. Abidi, Direct-conversion radio transceivers for digital communications, IEEE J.solid-state cir. 30 (12) (1995) 1399–1410.

[19] S. Mirabbasi, K. Martin, Classical and modern receiver architectures, IEEE Commun. Mag. 38 (11) (2000) 132–139.

[20] B. Selim, S. Muhaidat, P. C. Sofotasios, B. S. Sharif, T. Stouraitis, G. K. Karagiannidis, N. Al-Dhahir, Outage probability of single carrier NOMA systems under I/Q imbalance, in: 2018 IEEE Wirel. Commun. Net. Conf. (WCNC), IEEE, 2018, pp. 1–6.

[21] Ö. Özdemir, R. Hamila, N. Al-Dhahir, Exact average OFDM subcarrier SINR analysis under joint transmit–receive I/Q imbalance, IEEE Trans. Veh. Tech. 63 (8) (2014) 4125–4130.

[22] B. Selim, S. Muhaidat, P. C. Sofotasios, B. S. Sharif, T. Stouraitis, G. K. Karagiannidis, N. Al-Dhahir, Performance analysis of single carrier coherent and noncoherent modulation under I/Q imbalance, in: 2018 IEEE 87th Veh. Tech. Conf. (VTC Spring), IEEE, 2018, pp. 1–5.

[23] A.-A. A. Boulogeorgos, P. C. Sofotasios, B. Selim, S. Muhaidat, G. K. Karagiannidis, M. Valkama, Outage probability under I/Q imbalance and cascaded fading effects, in: 2016 23rd Intern. Conf. Tel. (ICT), IEEE, 2016, pp. 1–5.

[24] J. Li, M. Matthaiou, T. Svensson, I/Q imbalance in AF dual-hop relaying: Performance analysis in Nakagami-m fading, IEEE Trans. Commun. 62 (3) (2014) 836–847.

[25] X. Li, M. Liu, C. Deng, P. T. Mathiopoulos, Z. Ding, Y. Liu, Full-duplex cooperative NOMA relaying systems with I/Q imbalance and imperfect SIC, IEEE Wirel. Commun. Lett. 9 (1) (2019) 17–20.

[26] X. Li, M. Zhao, X.-C. Gao, L. Li, D.-T. Do, K. M. Rabie, R. Kharel, Physical layer security of cooperative NOMA for IoT networks under I/Q imbalance, IEEE Access 8 (2020) 51189–51199.

[27] H. Guo, X. Guo, C. Deng, S. Zhao, Performance analysis of IQI impaired cooperative NOMA for 5G-enabled Internet of Things, Wirel. Commun. Mob. Comp. 2020 (2020).

[28] X. Li, M. Zhao, C. Zhang, W. U. Khan, J. Wu, K. M. Rabie, R. Kharel, Security analysis of multi-antenna NOMA networks under I/Q imbalance, Electronics 8 (11) (2019) 1327.

[29] D. Cui, X. Li, G. Huang, K. Rabie, G. Nauryzbayev, B. M. ElHalawany, Outage Probability of ABCom NOMA Systems for 6G with IQI and RHIs, in: 2022 13th International Symposium on Communication Systems, Networks and Digital Signal Processing (CSNDSP), IEEE, 2022, pp. 384–389.

[30] D. Cui, G. Huang, Y. Zheng, H. Guo, J. Li, X. Li, Performance analysis of ABCom NOMA systems for 6G with generalized hardware impairments, Physical Communication 54 (2022) 101851.

[31] X. Li, M. Zhao, Y. Liu, L. Li, Z. Ding, A. Nallanathan, Secrecy analysis of ambient backscatter NOMA systems under I/Q imbalance, IEEE Transactions on Vehicular Technology 69 (10) (2020) 12286–12290.

[32] X. Li, Y. Zheng, M. D. Alshehri, L. Hai, V. Balasubramanian, M. Zeng, G. Nie, Cognitive AmBC-NOMA IoV-MTS networks with IQI: reliability and security analysis, IEEE Transactions on Intelligent Transportation Systems (2021).

[33] M. M. Alsmadi, N. A. Ali, M. Hayajneh, S. S. Ikki, Down-link NOMA networks in the presence of IQI and imperfect SIC: Receiver design and performance analysis, IEEE Transactions on Vehicular Technology 69 (6) (2020) 6793–6797.

[34] L. Bariah, B. Selim, L. Mohjazi, S. Muhaidat, P. C. Sofotasios, W. Hamouda, Pairwise error probability of non-orthogonal multiple access with I/Q imbalance, in: 2019 UK/China Emerging Technologies (UCET), IEEE, 2019, pp. 1–4.

[35] A.-A. A. Boulogeorgos, V. M. Kapinas, R. Schober, G. K. Karagiannidis, I/Q-imbalance self-interference coordination, IEEE Transactions on Wireless Communications 15 (6) (2016) 4157–4170.

[36] L. Anttila, M. Valkama, M. Renfors, Circularity-based I/Q imbalance compensation in wideband direct-conversion receivers, IEEE Transactions on Vehicular Technology 57 (4) (2008) 2099–2113.

[37] B. Razavi, RF microelectronics, Upper Saddle River, NJ, USA: Prentice-Hall, Inc (1998.).

[38] A.-A. A. Boulogeorgos, P. C. Sofotasios, B. Selim, S. Muhaidat, G. K. Karagiannidis, M. Valkama, Effects of RF impairments in communications over cascaded fading channels, IEEE Trans. Veh. Tech. 65 (11) (2016) 8878–8894.

[39] S. Valentin, D. H. Woldegebreal, T. Volkhausen, H. Karl, Combining for cooperative WLANs-a reality check based on prototype measurements, in: 2009 IEEE Intern. Conf. Commun. Workshops, IEEE, 2009, pp. 1–5.